Shear-Induced Alignment of Nonspherical Brownian Particles Near Walls

Johannes M. Nitsche and Partha Roy
Dept. of Chemical Engineering, State University of New York at Buffalo, Buffalo, NY 14260

A theoretical investigation is presented of the convection-diffusion of model nonspherical solutes in shear flow over a plane wall. The analysis proceeds by formulating the underlying configuration-space Brownian transport equation for the distribution over accessible positions and orientations. Geometrical constraints are imposed via boundary conditions preventing wall penetration, and some of the calculations incorporate hydrodynamic interactions with the wall. The analysis is brought to fruition by regular perturbation expansion in the rotary Péclet number, and solution of the resultant boundary-value problems by a Galerkin technique. Three specific mechanistic conclusions result from the analysis. First, steric constraints imposed by the wall impedes the shear-induced solute alignment (producing a more nearly uniform distribution over orientations relative to the unbounded-fluid case) near the wall. Second, although the first effect of flow is to counteract the equilibrium depletion of solute centers near the wall, flow reinforces this depletion at higher order in the shear rate. Third, solute-wall hydrodynamic interactions act to strengthen the shear-induced solute alignment near the wall. This last phenomenon occurs because hydrodynamic wall effects significantly decrease the rotary diffusivity, but have little effect on the angular velocity, thereby locally increasing the effective rotary Péclet number (the effective flow strength). Correspondingly, solute-wall hydrodynamic interactions reinforce the flow effects on the near-wall depletion just noted. Steric and hydrodynamic wall effects typically are of order 15–20% near the wall.

Introduction

The hindered convection of macromolecules and colloidal particles near surfaces and through pores is central to numerous separations and rheological processes, including hydrodynamic chromatography (DiMarzio and Guttman, 1970; Prud'homme et al., 1982; McHugh, 1984), field-flow fractionation (Giddings, 1984–1985), and the flow of polymer solutions through porous media (Aubert and Tirrell, 1982; Chauveteau, 1982). The confined Brownian motion of roughly spherical solutes is largely understood, at least in simple pore geometries (McHugh, 1984), as is the dynamics of nonspherical particle transport in unbounded flows (Bird and Warner, 1971; Hinch and Leal, 1972; Stewart and Sorensen, 1972). However, many questions remain open regarding the convection of *nonspherical* Brownian solutes *near walls*. For such species, both flow-induced alignment and geometrical constraints imposed by bounding surfaces impact materially on distributions over molecular orientations and on dissipation rates. Thus, the theoretical study of such effects at the microscopic scale is key to the interpretation and detailed understanding of measured transport and rheological properties.

In hydrodynamic chromatographic experiments that compare the elution characteristics of latex spheres and the rod-like xanthan polysaccharide, Prud'homme et al. (1982) present strong evidence for flow-induced molecular alignment. These experimental findings are supported by order-of-magnitude calculations based on orientational distributions for *unbounded* linear flows, which show that the apparent degree of alignment is roughly consistent with rates of shear and elongation estimated to occur within the porous packing (Prud'homme and Hoagland, 1983).

Within rheological contexts, more detailed theoretical analyses have been undertaken to understand the interplay between such flow-induced alignment (and stretching) and the steric constraints imposed by bounding walls, the latter ignored by Prud'homme and Hoagland (1983). Kinetic theory for flexible (bead-spring) dumbbell models of polymers is well

developed, at least for the case of point-size beads that do not interact hydrodynamically with the walls or with each other (e.g., Goh et al., 1985a,b; Brunn and Grisafi, 1987a,b; Grisafi and Brunn, 1989). By comparison, relatively little work has addressed rigid solutes. In their study, *inter alia*, of the convection-diffusion of a rigid point-bead dumbbell in Poiseuille flow within a slit pore, Stasiak and Cohen (1983) develop a perturbation expansion for the distribution over positions and orientations in powers of the rotary Péclet number (assumed small). Although they draw rheological conclusions from this expansion relating to spatial inhomogeneity of the shear rate, their analysis is based upon a boundary condition that prevents only the center of mass, but not the beads, from penetrating the walls. In their corresponding analysis of simple shear flow, Park and Fuller (1984) account for the wall contact geometry, and so explicitly incorporate the fact that rotation is constrained when the dumbbell center lies within one half-length of the walls. However, their calculations are based upon an incomplete boundary condition that precludes only diffusive flux through the walls, but not convective flux. Thus, both analyses effectively address only the bulk-flow physics and leave completely open the dynamical processes by which the walls affect rotation.

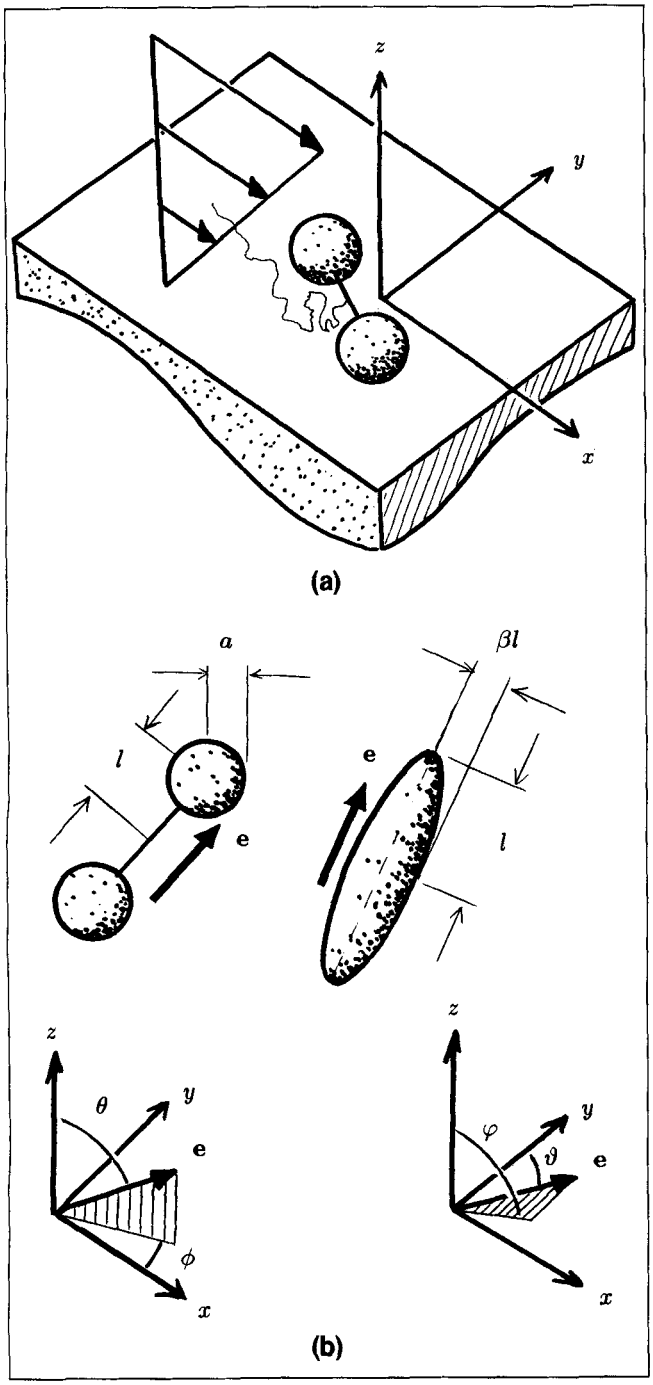

Figure 1. Definition sketch: (a) nonspherical particle in simple shear flow over a planar wall; (b) two alternate parametrizations of the particle orientation.

Recent theoretical developments on Brownian motion near walls (Nitsche and Brenner, 1990; Nitsche, 1991) have established a general framework for the construction of boundary conditions expressing wall impenetrability for rigid solutes of arbitrary shape. Using this framework, Schiek and Shaqfeh (1995) for the first time account properly for the near-wall physics in their calculation of the first two terms in a small Péclet number expansion of the distribution over positions and orientations. This calculation of the configurational distribution is coupled with a comprehensive general theory of nonlocal stress effects for suspensions of thin rods in simple shear and Poiseuille flows between flat plates. De Pablo et al. (1992) present a corresponding study on the distribution of rigid dumbbells and multibead rods in simple shear flow between flat plates via Brownian dynamics simulation. Both analyses account for hydrodynamic anisotropy of a rodlike solute, but ignore its hydrodynamic interaction with the walls. Conclusions of this previous work are considered vis-à-vis the present analysis in the "Discussion" section.

The purpose of this article is to advance the understanding of confined convection-diffusion of rigid nonspherical solutes by studying further effects of steric (geometrical) constraints on flow-induced alignment and by incorporating hydrodynamic interactions to ascertain the manner in which hydrodynamic wall effects influence the configurational distribution. This program is pursued with reference to the motion of simple model solutes in shear flow over a planar wall. The next section develops the pertinent Brownian transport equations. Subsequently, we introduce approximate expressions for the requisite configuration-dependent diffusion and velocity components, and devise a numerical solution procedure. These developments are ultimately applied to calculate distributions over accessible solute positions and orientations.

Formulation of the Model Problem

The physical system in Figure 1a consists of a semiinfinite expanse of fluid undergoing simple shear flow in the positive x direction above a rigid plane wall at $z = 0$, for which the velocity field is

$$u(x) = i\dot{\gamma}z. \tag{1}$$

Suspended in this flow is a rigid nonspherical particle that in our analysis is taken to be one of two simple model particles:

(1) a dumbbell composed of two freely rotating spherical beads of radius a separated by a rigid connector (with negli-

gible hydrodynamic resistance) holding their centers at a fixed distance $2l$, or

(2) a prolate spheroid with major semiaxis l and minor semiaxis βl.

In both cases, the solute configuration is quantified by the position coordinates $\boldsymbol{x} \Leftrightarrow (x, y, z)$ of its center and by polar and azimuthal angles $\boldsymbol{e} \Leftrightarrow (\theta, \phi)$, respectively measured from the z and x axes, specifying the direction of its axis of revolution (Figure 1b). Since the solute particle cannot penetrate the solid wall, the set of vertical positions accessible to its center depends upon the polar angle θ (cf. Hoagland, 1988; Park and Fuller, 1984; Schiek and Shaqfeh, 1995). Thus, the configuration must lie within the accessible set

$$\Omega^{xe} = \{(x, y, z, \theta, \phi) : (z, \theta) \in \Omega^{z\theta}\},$$

$$\Omega^{z\theta} = \{(z, \theta) : S(z, \theta) \geq 0\} \quad \text{with}$$

$$S(z, \theta) = z/l - \alpha - \sqrt{\cos^2\theta + \beta^2 \sin^2\theta}, \quad (2)$$

where $\alpha \equiv a/l$. In Eq. 2, β is set to zero in considering the case of a dumbbell, and a is likewise set to zero for the case of a spheroid.

In interpreting the results below, it will be useful in certain cases to introduce an alternative set (ϑ, φ) of polar and azimuthal angles, respectively measured from the y and z axes, as indicated in Figure 1b, following more closely the conventions usual in analyses of rotary transport in unbounded shear flows (cf. Hinch and Leal, 1972; Stewart and Sorensen, 1972). The two sets of angles are related by the expressions

$$\cos\vartheta = \sin\theta \sin\phi,$$

$$\sin\vartheta \cos\varphi = \cos\theta. \quad (3)$$

Steady-state Brownian motion of the solute is described by a probability density $P(x, y, z, \theta, \phi)$ giving the distribution over positions and orientations. Attention is focused upon an x- and y-independent distribution, which is governed by the transport equation (Brenner and Condiff, 1972; Nitsche and Brenner, 1990)

$$\nabla_z \cdot {}^z\boldsymbol{J} + \nabla_e \cdot {}^e\boldsymbol{J} = 0 \quad (4)$$

posed in Ω^{ze}, in which the translational and rotational fluxes are given by the convective-diffusive constitutive relations

$${}^z\boldsymbol{J} = -{}^{zz}\mathsf{D} \cdot \nabla_z P - {}^{ez}\mathsf{D}^\dagger \cdot \nabla_e P + (\boldsymbol{k}\dot{z})P,$$

$${}^e\boldsymbol{J} = -{}^{ez}\mathsf{D} \cdot \nabla_z P - {}^{ee}\mathsf{D} \cdot \nabla_e P + \dot{\boldsymbol{e}}P. \quad (5)$$

In these equations, ∇_z and ∇_e, respectively, denote the translational and rotational gradient operators

$$\nabla_z = \boldsymbol{k}\partial/\partial z, \quad \nabla_e = \boldsymbol{i}_\theta \partial/\partial\theta + \boldsymbol{i}_\phi (\sin\theta)^{-1} \partial/\partial\phi. \quad (6)$$

The dyadics ${}^{zz}\mathsf{D}$, ${}^{ee}\mathsf{D}$, and ${}^{ez}\mathsf{D}$ denote the diffusion dyadics for (z-directed) translation, for rotation, and for coupling between these modes of motion. The vectors $\boldsymbol{k}\dot{z}$ and $\dot{\boldsymbol{e}}$ represent the force- and torque-free translational and angular velocities of the freely suspended solute. It is worth noting that

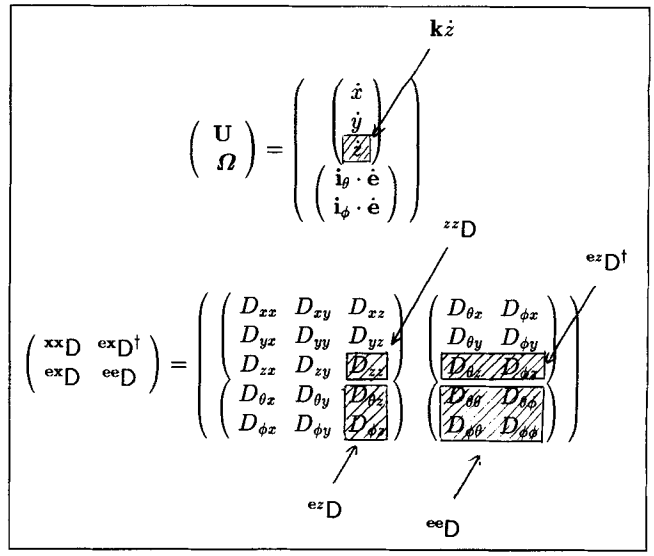

Figure 2. Partitioning of the grand diffusion dyadic and particle velocity vector.

${}^{zz}\mathsf{D}$, ${}^{ez}\mathsf{D}$, and $\boldsymbol{k}\dot{z}$, respectively, constitute subblocks of the corresponding full translational diffusivity, coupling diffusivity, and translational velocity, as indicated in Figure 2.

Impenetrability of the wall is maintained by imposing the boundary condition

$$(\nabla_z S) \cdot {}^z\boldsymbol{J} + (\nabla_e S) \cdot {}^e\boldsymbol{J} = 0 \quad (7)$$

at the surface given by $S(z, \theta) = 0$, which expresses the fact that translational and rotational fluxes must conspire to produce zero net solute flux through the wall ($z = 0$) at its point of contact with the wall; Eq. 7 can also be interpreted as requiring zero normal flux at the boundary $\partial\Omega^{ze}$ of the configuration space corresponding to solute-wall contact (Nitsche and Brenner, 1990; Nitsche, 1991). Far from the wall the z-directed particle flux must decay to zero at all orientations, so that

$$\boldsymbol{k} \cdot {}^z\boldsymbol{J} \to 0 \quad \text{as} \quad z \to \infty. \quad (8)$$

The scale of the solution is set arbitrarily by requiring P to relax to the normalized orientational distribution $P_\infty(\boldsymbol{e})$ for an unbounded shear flow:

$$P(z, \boldsymbol{e}) \to P_\infty(\boldsymbol{e}) \quad \text{as} \quad z \to \infty. \quad (9)$$

Additionally, P must satisfy conditions at boundedness (owing to Legendre-type singularities in the transport equation at $\theta = 0$ and π) and of periodicity in ϕ.

Hydrodynamic Coefficients

To assess the manner in which hydrodynamic wall effects influence the distribution over positions and orientations, it is necessary to calculate diffusivities and convective velocities characterizing solute motion near a plane wall at vanishing Reynolds number. The two model particles considered here are prototypical solutes for which this task can accomplish a reasonable approximation in a rather explicit form.

Dumbbell

For the dumbbell (assumed to have freely rotating beads) in quiescent fluid, the hydrodynamic forces on the "+" and "−" beads are linearly related to their respective velocities $\boldsymbol{U}_+$ and $\boldsymbol{U}_-$ via expressions of the form

$$\boldsymbol{F}_+ = -6\pi\mu a(\mathsf{k}_{++}\cdot\boldsymbol{U}_+ + \mathsf{k}_{+-}\cdot\boldsymbol{U}_-),$$
$$\boldsymbol{F}_- = -6\pi\mu a(\mathsf{k}_{-+}\cdot\boldsymbol{U}_+ + \mathsf{k}_{--}\cdot\boldsymbol{U}_-). \quad (10)$$

The positions $\boldsymbol{x}_+$, $\boldsymbol{x}_-$ and velocities $\boldsymbol{U}_+$, $\boldsymbol{U}_-$ of the beads are of course not independent, being related by the expressions

$$\boldsymbol{x}_\pm = \boldsymbol{x} \pm l\boldsymbol{e},$$
$$\boldsymbol{U}_\pm = \boldsymbol{U} \mp l\mathsf{a}\cdot\boldsymbol{\Omega}, \quad (11)$$

with $\boldsymbol{x}$ the position of the dumbbell center, $\boldsymbol{U}$ its velocity, and $\boldsymbol{\Omega}$ the angular velocity. Here a denotes the dyadic

$$\mathsf{a} = \boldsymbol{i}_\phi\boldsymbol{i}_\theta - \boldsymbol{i}_\theta\boldsymbol{i}_\phi. \quad (12)$$

In terms of the preceding quantities, the translational, rotational and coupling resistance dyadics of the dumbbell are:

$$(6\pi a)^{-1\,t}\mathsf{K} \equiv {}^t\mathsf{k} = \mathsf{k}_{++} + \mathsf{k}_{+-} + \mathsf{k}_{-+} + \mathsf{k}_{--},$$
$$(6\pi a l)^{-1\,c}\mathsf{K} \equiv {}^c\mathsf{k} = \mathsf{a}\cdot(\mathsf{k}_{++} + \mathsf{k}_{+-} - \mathsf{k}_{-+} - \mathsf{k}_{--}),$$
$$(6\pi a l^2)^{-1\,r}\mathsf{K} \equiv {}^r\mathsf{k} = \mathsf{a}\cdot(\mathsf{k}_{+-} - \mathsf{k}_{++} - \mathsf{k}_{--} + \mathsf{k}_{-+})\cdot\mathsf{a}. \quad (13)$$

A reasonable approximation for hydrodynamic interaction effects is obtained by taking (1) the direct resistance dyadics k_{++} and k_{--} to be synonymous with the (dimensionless) resistance dyadics for translation of isolated spheres near a plane wall, that is

$$\mathsf{k}_{\pm\mp} = (\boldsymbol{ii} + \boldsymbol{jj})F_\parallel(z_\pm/a) + \boldsymbol{kk}F_\perp(z_\pm/a), \quad (14)$$

and (2) the cross-resistance dyadics to be given by Stokeslet interactions, namely,

$$\mathsf{k}_{\pm\mp} = -6\pi\mu a\mathsf{V}^p(\boldsymbol{x}_\pm;\boldsymbol{x}_\mp) \quad (15)$$

(cf. Nitsche, 1995). In these equations, $F_\parallel$ and $F_\perp$ represent dimensionless resistance coefficients for motion parallel and perpendicular to the wall, collectively tabulated by Brenner (1961), Goldman et al. (1967a), and Falade and Brenner (1988) as functions of the elevation z of the sphere center in units of the sphere radius a (see the Appendix). The dyadic $\mathsf{V}^p(\boldsymbol{x};\boldsymbol{x}_0)$ represents the fundamental singular solution of the Stokes equations having singularity at $\boldsymbol{x}_0$ and satisfying the no-slip condition on the plane $z=0$, given by Blake (1971); cf. Nitsche (1995). The expression for ${}^r\mathsf{K}$ in Eq. 13 produces zero resistance for rotation about the axis. A term proportional to the dyadic $\boldsymbol{ee}$ must therefore be appended to prevent ${}^r\mathsf{K}$ from being singular, but the resistance coefficient for rotation about the axis (representing a dead degree of freedom (Condiff and Dahler, 1966)) disappears from the axisymmetric ('e-form') diffusivities ${}^{ez}\mathsf{D}$ and ${}^{ee}\mathsf{D}$ computed from the identities in Eq. 27, as it must.

In shear flow past a stationary dumbbell, the hydrodynamic forces on the beads are given by the corresponding approximations

$$\boldsymbol{F}_+ = 6\pi\mu a\dot\gamma l[\boldsymbol{i}(z_+/l)F_s(z_+/a) + (z_-/l)\mathsf{k}_{+-}\cdot\boldsymbol{i}],$$
$$\boldsymbol{F}_- = 6\pi\mu a\dot\gamma l[\boldsymbol{i}(z_-/l)F_s(z_-/a) + (z_+/l)\mathsf{k}_{-+}\cdot\boldsymbol{i}], \quad (16)$$

with F_s the dimensionless hydrodynamic force on an isolated, freely rotating (but stationary) sphere in shear flow over a plane wall, calculable from the tabulation of Goldman et al., (1967b) (see Appendix). Starting from a superposition of Eqs. 10 and 16 for the general case where the dumbbell moves in the flow, and setting the total hydrodynamic force and torque on it equal to zero (so that it is freely suspended), straightforward manipulations lead to the following expressions for its shear-driven translational and angular velocities:

$$(\dot\gamma l)^{-1}\boldsymbol{U} = ({}^t\mathsf{k} - {}^c\mathsf{k}^\dagger\cdot{}^r\mathsf{k}^{-1}\cdot{}^c\mathsf{k})^{-1}\cdot(\Sigma - {}^c\mathsf{k}^\dagger\cdot{}^r\mathsf{k}^{-1}\cdot\mathsf{a}\cdot\Delta)\cdot\boldsymbol{i},$$
$$\dot\gamma^{-1}\boldsymbol{\Omega} = ({}^r\mathsf{k} - {}^c\mathsf{k}\cdot{}^t\mathsf{k}^{-1}\cdot{}^c\mathsf{k}^\dagger)^{-1}\cdot(\mathsf{a}\cdot\Delta - {}^c\mathsf{k}\cdot{}^t\mathsf{k}^{-1}\cdot\Sigma)\cdot\boldsymbol{i}, \quad (17)$$

where

$$\Sigma = l[(z_+/l)F_s(z_+/a) + (z_-/l)F_s(z_-/a)] + (z_-/l)\mathsf{k}_{+-} + (z_+/l)\mathsf{k}_{-+},$$
$$\Delta = l[(z_+/l)F_s(z_+/a) - (z_-/l)F_s(z_-/a)] + (z_-/l)\mathsf{k}_{+-} - (z_+/l)\mathsf{k}_{-+}. \quad (18)$$

Calculations below are based on the arbitrary choice of bead radius $a = 0.2l$ for illustrative purposes.

Spheroid

For a spheroidal solute, we shall be content to utilize asymptotic expressions based upon the method of reflections carried out through second order in powers of the solute length l divided by its distance to the wall z, as given in most comprehensive form by Hirschfeld et al. (1984). Although this far-field approximation does not, of course, strictly apply when the spheroid lies within $O(l)$ distances from the wall, it is in fact reasonably accurate quantitatively at such distances. This statement can be verified by comparison with recent boundary-integral calculations reported by Hsu and Ganatos (1989). The various diffusion coefficients are found to decrease with decreasing distance from the wall, albeit not exactly to zero as dictated by the lubrication singularity at near-contact configurations. The region in which the diffusivities are seriously in error, however, amounts to a relatively thin layer near the boundary $S(\boldsymbol{x},\boldsymbol{e}) = 0$ of the accessible configuration space. Although our hydrodynamic calculations for the spheroid certainly underestimate the severity of hindrance effects near the wall, the quantitative errors incurred should not impact the veracity of our qualitative conclusions.

The resistance dyadics are given by the following expressions after Hirschfeld et al. (1984) with slight notational changes:

$$(6\pi l)^{-1}{}^{t}\mathsf{K} \equiv {}^{t}\mathsf{k} = {}^{t}\mathsf{k}_{\infty}\cdot\left[\mathsf{I}-(l/z)\mathsf{W}\cdot{}^{t}\mathsf{k}_{\infty}\right]^{-1},$$

$$(6\pi l^2)^{-1}{}^{c}\mathsf{K} \equiv {}^{c}\mathsf{k} = (4/3)(l/z)^2\Gamma_{\infty}:(\nabla\mathsf{W})\cdot{}^{t}\mathsf{k}_{\infty},$$

$$(6\pi l^3)^{-1}{}^{r}\mathsf{K} \equiv {}^{r}\mathsf{k} = (4/3)\Gamma_{\infty}:\epsilon. \tag{19}$$

Here, ${}^{t}\mathsf{k}_{\infty}$ denotes the dimensionless unbounded-fluid translational resistance dyadic, given by

$$(6\pi l)^{-1}{}^{t}\mathsf{K}_{\infty} \equiv {}^{t}\mathsf{k}_{\infty} = \boldsymbol{ee}G_{\parallel} + (\mathsf{I}-\boldsymbol{ee})G_{\perp}, \tag{20}$$

and Γ_{∞} similarly denotes the unbounded-fluid rotational triadic

$$\Gamma_{\infty} = \left(\boldsymbol{i}_{\phi}\boldsymbol{i}_{\theta}\boldsymbol{e} - \boldsymbol{i}_{\theta}\boldsymbol{i}_{\phi}\boldsymbol{e} + \beta^2\boldsymbol{i}_{\theta}\boldsymbol{e}\boldsymbol{i}_{\phi} - \beta^2\boldsymbol{i}_{\phi}\boldsymbol{e}\boldsymbol{i}_{\theta}\right)\frac{H_{\perp}}{1+\beta^2} + (\boldsymbol{e}\boldsymbol{i}_{\phi}\boldsymbol{i}_{\theta} - \boldsymbol{e}\boldsymbol{i}_{\theta}\boldsymbol{i}_{\phi})\frac{H_{\parallel}}{2}; \tag{21}$$

both depend upon the particle orientation as embodied in the orthonormal triad $\{\boldsymbol{i}_{\theta}, \boldsymbol{i}_{\phi}, \boldsymbol{e}\}$. The quantity $\epsilon = -\mathsf{I}\times\mathsf{I}$ represents the unit isotropic pseudotriadic (Hirschfeld et al., 1984). Equation 21 has been written in such a way that $H_{\parallel}$ and $H_{\perp}$ represent the dimensionless unbounded-fluid rotational resistances of the spheroid. Thus, according to the third member of Eq. 19,

$$(8\pi l^3)^{-1}{}^{r}\mathsf{K} = \boldsymbol{ee}H_{\parallel} + (\mathsf{I}-\boldsymbol{ee})H_{\perp}. \tag{22}$$

It is worth noting that, through second order in the reflection scheme, the rotational resistance itself is unaffected by hydrodynamic interactions with the walls. This is *not* to say, however, that particle rotation is free from a hydrodynamic wall effect—see, for example, the angular velocity given by Eq. 24 below, in which ${}^{t}\mathsf{k}$ and ${}^{c}\mathsf{k}$ depend upon z. The quantities W and $\nabla\mathsf{W}$ represent wall-effect tensors given explicitly by (cf. Brenner, 1962; Happel and Brenner, 1991, p. 341; Hirschfeld et al., 1984; Falade and Brenner, 1985):

$$\mathsf{W} = (\boldsymbol{ii}+\boldsymbol{jj})(9/16) + \boldsymbol{kk}(9/8),$$

$$\nabla\mathsf{W} = -\boldsymbol{kkk}(9/16) + (\boldsymbol{iik} - \boldsymbol{kii} - \boldsymbol{iki} + \boldsymbol{jjk} - \boldsymbol{kjj} - \boldsymbol{jkj})(9/32). \tag{23}$$

The force- and torque-free translational velocities are given by the equations

$$(\dot{\gamma}l)^{-1}\boldsymbol{U} = \boldsymbol{i}(z/l) - (4/3)({}^{t}\mathsf{k} - {}^{c}\mathsf{k}^{\dagger}\cdot{}^{r}\mathsf{k}^{-1}\cdot{}^{c}\mathsf{k})^{-1}\cdot{}^{c}\mathsf{k}^{\dagger}\cdot{}^{r}\mathsf{k}^{-1}\cdot\Gamma_{\infty}:\boldsymbol{ki},$$

$$\dot{\gamma}^{-1}\Omega = (4/3)({}^{r}\mathsf{k} - {}^{c}\mathsf{k}\cdot{}^{t}\mathsf{k}^{-1}\cdot{}^{c}\mathsf{k}^{\dagger})^{-1}\cdot\Gamma_{\infty}:\boldsymbol{ki}, \tag{24}$$

obtained by setting the hydrodynamic force and torque on the spheroid in shear flow (cf. Hirschfeld et al., 1984) equal to zero.

Calculations below are based on the arbitrary choice of aspect ratio $\beta = 0.1$ for illustrative purposes. A spheroid with this aspect ratio is characterized by the numerical values (cf. Happel and Brenner, 1991, p. 223; Hirschfeld et al., 1984; Hsu and Ganatos, 1989)

$$G_{\parallel} = 0.2647, \quad G_{\perp} = 0.3812, \quad H_{\parallel} = 0.0068, \quad H_{\perp} = 0.1337. \tag{25}$$

Calculation of diffusivity and velocity components

For both model particles, the diffusion dyadics are related to the resistance dyadics (approximated as described above) via the Einstein relation

$$\begin{pmatrix} {}^{t}\mathsf{D} & {}^{c}\mathsf{D}^{\dagger} \\ {}^{c}\mathsf{D} & {}^{r}\mathsf{D} \end{pmatrix} = \frac{kT}{\mu}\begin{pmatrix} {}^{t}\mathsf{K} & {}^{c}\mathsf{K}^{\dagger} \\ {}^{c}\mathsf{K} & {}^{r}\mathsf{K} \end{pmatrix} \tag{26}$$

The entries in the axisymmetric-form particle diffusivities ${}^{zz}\mathsf{D}$, ${}^{ez}\mathsf{D}$, ${}^{ee}\mathsf{D}$ can be obtained from the invariant-form diffusivities ${}^{t}\mathsf{D}$, ${}^{c}\mathsf{D}$, ${}^{r}\mathsf{D}$ via the equations (see Nitsche and Brenner, 1990)

$${}^{zz}\mathsf{D} = \boldsymbol{kk}(\boldsymbol{k}\cdot{}^{t}\mathsf{D}\cdot\boldsymbol{k}),$$

$${}^{ez}\mathsf{D} = \boldsymbol{i}_{\theta}\boldsymbol{k}(\boldsymbol{i}_{\phi}\cdot{}^{c}\mathsf{D}\cdot\boldsymbol{k}) - \boldsymbol{i}_{\phi}\boldsymbol{k}(\boldsymbol{i}_{\theta}\cdot{}^{c}\boldsymbol{D}\cdot\boldsymbol{k}),$$

$${}^{ee}\mathsf{D} = \boldsymbol{i}_{\theta}\boldsymbol{i}_{\theta}(\boldsymbol{i}_{\phi}\cdot{}^{r}\mathsf{D}\cdot\boldsymbol{i}_{\phi}) - \boldsymbol{i}_{\theta}\boldsymbol{i}_{\phi}(\boldsymbol{i}_{\phi}\cdot{}^{r}\mathsf{D}\cdot\boldsymbol{i}_{\theta}) - \boldsymbol{i}_{\phi}\boldsymbol{i}_{\theta}(\boldsymbol{i}_{\theta}\cdot{}^{r}\mathsf{D}\cdot\boldsymbol{i}_{\phi}) + \boldsymbol{i}_{\phi}\boldsymbol{i}_{\phi}(\boldsymbol{i}_{\theta}\cdot{}^{r}\mathsf{D}\cdot\boldsymbol{i}_{\theta}). \tag{27}$$

Also,

$$\dot{\boldsymbol{kz}} = \boldsymbol{k}(\boldsymbol{k}\cdot\boldsymbol{U}),$$

$$\dot{\boldsymbol{e}} = \boldsymbol{i}_{\theta}(\boldsymbol{i}_{\phi}\cdot\Omega) - \boldsymbol{i}_{\phi}(\boldsymbol{i}_{\theta}\cdot\Omega), \tag{28}$$

the latter equation deriving from the identity $\dot{\boldsymbol{e}} = -\boldsymbol{e}\times\Omega$ (Brenner and Condiff, 1972). It is worth noting that $\dot{z}\to 0$ as $z\to\infty$.

Figures 3 and 4 show the angular dependencies of selected velocity and diffusivity components for the dumbbell and spheroid, respectively, in the plane of shear ($\vartheta = \pi/2$) at fixed elevation z. In order to distinguish the effects of hydrodynamic interactions with the wall, we adopt a practice to be repeated below and compare the complete results (solid curves) with corresponding results where hydrodynamic wall effects have been artificially switched off (dot-dashed curves). (For the dumbbell, we achieve this switching off by setting $F_{\parallel}$, $F_{\perp}$, and F_s in Eqs. 14 and 16 to unity and by eliminating the reflected fields due to the walls in the Stokeslets appearing in Eq. 15; for the spheroid we set W and $\nabla\mathsf{W}$ in Eqs. 23 to zero.) For the dumbbell, additional curves are presented where bead–bead interactions have also been switched off by setting k_{+-} and k_{-+} to zero (dashed curves). By comparing dot-dashed and solid curves, it is seen that hydrodynamic wall effects have a small influence on the force- and torque-free angular velocity of the dumbbell (Figure 3a) but significantly decrease the rotary diffusivity (by about 15–20% at $z = 1.25l$—see Figure 3b. (The relatively small effect of solute–wall hydrodynamic interactions upon the angular velocity is consistent with the findings of Stover and Cohen (1990) and Ingber and Mondy (1994).) It is interesting to note that near $\varphi = 0$ shear-induced rotation is actually slightly enhanced as opposed to hindered. Hydrodynamic wall effects for rota-

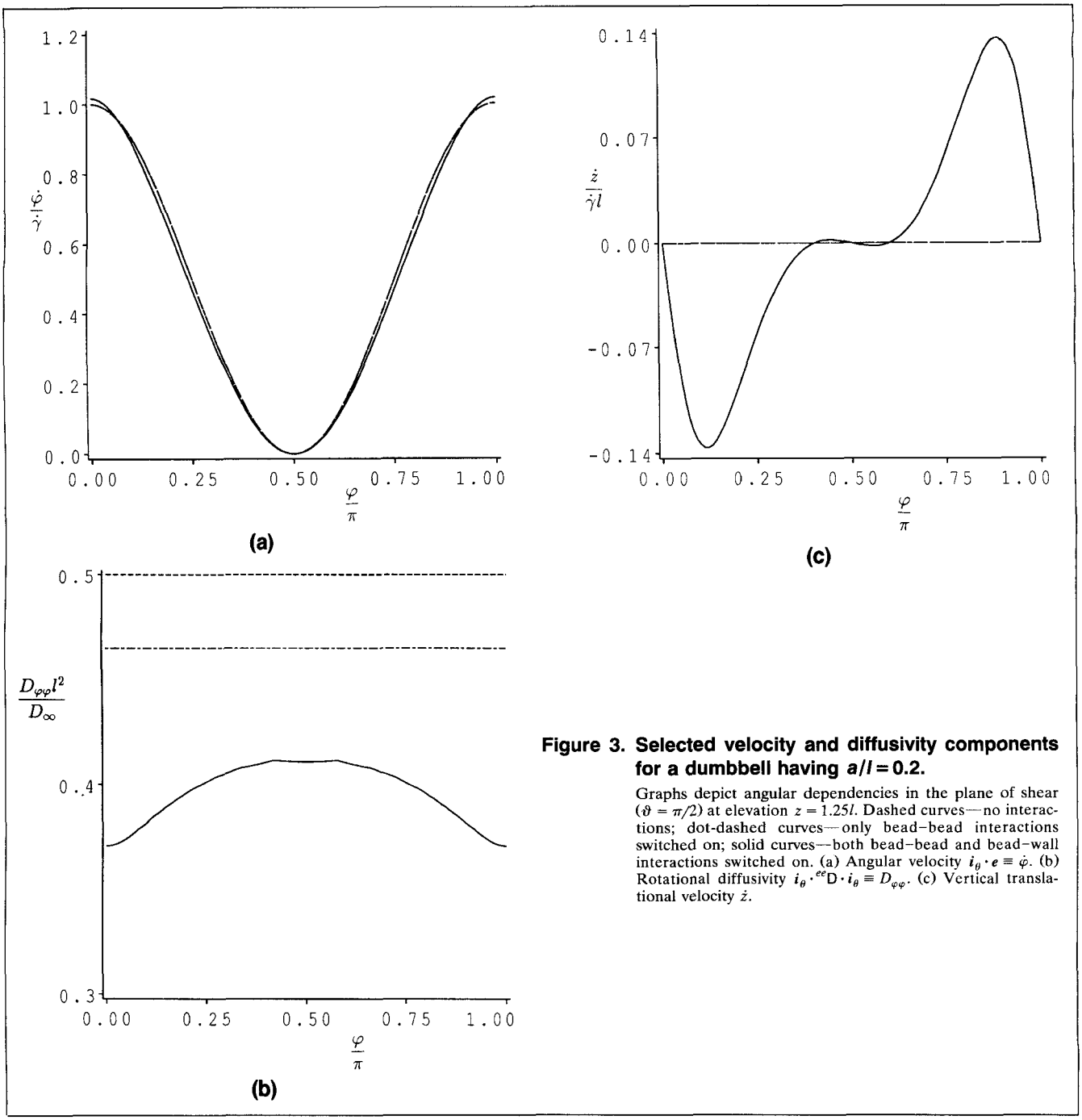

Figure 3. Selected velocity and diffusivity components for a dumbbell having $a/l = 0.2$.

Graphs depict angular dependencies in the plane of shear ($\vartheta = \pi/2$) at elevation $z = 1.25l$. Dashed curves—no interactions; dot-dashed curves—only bead–bead interactions switched on; solid curves—both bead–bead and bead–wall interactions switched on. (a) Angular velocity $\boldsymbol{i}_\theta \cdot \boldsymbol{e} \equiv \dot{\varphi}$. (b) Rotational diffusivity $\boldsymbol{i}_\theta \cdot {}^{ee}\mathsf{D} \cdot \boldsymbol{i}_\theta \equiv D_{\varphi\varphi}$. (c) Vertical translational velocity $\dot{z}$.

tional motions of the spheroid predicted by the second-order reflection theory (Figures 4a and 4b) must be regarded as tiny perturbations without significance. For both types of solute particle there exists a nonzero z-directed convective velocity (Figures 3c and 4c) owing to coupling between translational and rotational motions. In particular, for $0 < \varphi < \pi/2$ the greater resistance to vertical motion experienced by the lower (and lagging) bead or blunt end of the solute implies that rotation forces the center downwards, so that $\dot{z}$ is negative. (For the dumbbell, the slight oscillations of $\dot{z}$ above and below zero near $\varphi = \pi/2$ may be an artifact of the neglect of higher-order terms in the truncated reflection expansion underlying Eq. 17.)

Solution of the Transport Equation

Henceforth we shall work with dimensionless versions of the transport equations, which look identical to the dimensional versions, with the exception that the convective terms in Eq. 5 are multiplied by a Péclet number (Pe). The various dimensionless quantities are defined in terms of their dimensional counterparts (now distinguished with the prime $'$ superscript) according to the relations

$$z = z'/l,$$

$${}^{zz}\mathsf{D} = (D_\infty^{-1})\,{}^{zz}\mathsf{D}',$$

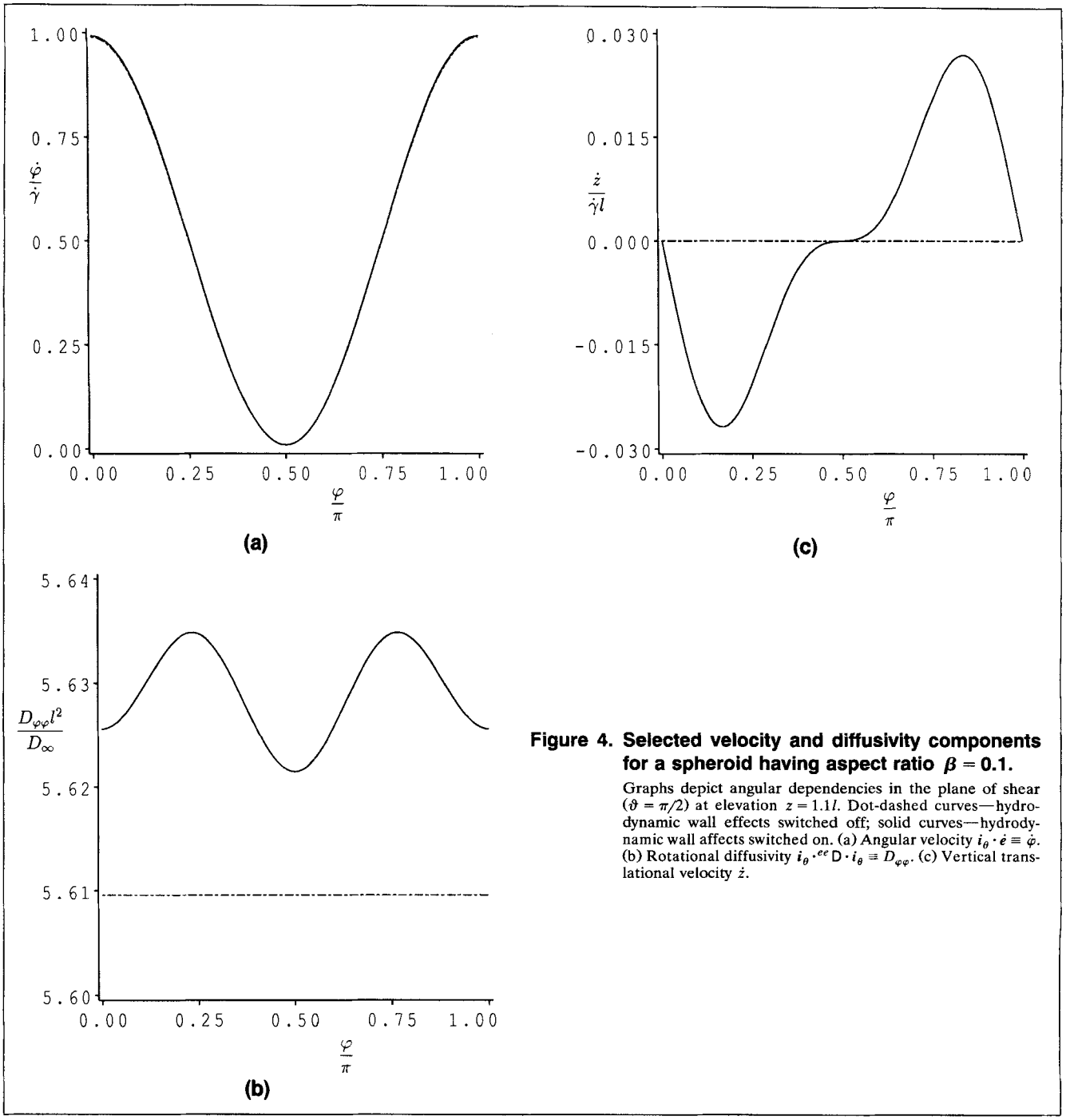

Figure 4. Selected velocity and diffusivity components for a spheroid having aspect ratio $\beta = 0.1$.

Graphs depict angular dependencies in the plane of shear ($\vartheta = \pi/2$) at elevation $z = 1.1l$. Dot-dashed curves—hydrodynamic wall effects switched off; solid curves—hydrodynamic wall affects switched on. (a) Angular velocity $\boldsymbol{i}_\theta \cdot \dot{\boldsymbol{e}} \equiv \dot{\varphi}$. (b) Rotational diffusivity $\boldsymbol{i}_\theta \cdot {}^{ee}\mathsf{D} \cdot \boldsymbol{i}_\theta \equiv D_{\varphi\varphi}$. (c) Vertical translational velocity $\dot{z}$.

$$
\begin{aligned}
{}^{ez}\mathsf{D} &= (l/D_\infty)\,{}^{ez}\mathsf{D}', \\
{}^{ee}\mathsf{D} &= (l^2/D_\infty)\,{}^{ee}\mathsf{D}', \\
\dot{z} &= (\dot{\gamma}l)^{-1}\dot{z}', \\
\dot{\boldsymbol{e}} &= (\dot{\gamma})^{-1}\dot{\boldsymbol{e}}'.
\end{aligned} \tag{29}
$$

Here D_∞ represents a number of order the unbounded-fluid translational diffusivity; specifically, we take

$$
D_\infty = \begin{cases} kT/6\pi\mu a & \text{(dumbbell)}, \\ kT/6\pi\mu l & \text{(spheroid)}. \end{cases} \tag{30}
$$

The Péclet number

$$
Pe = \dot{\gamma}l^2/D_\infty \tag{31}
$$

appearing in subsequent equations has the significance of a rotational Péclet number.

We shall seek an approximate solution of the preceding equations in the form of the $Pe \ll 1$ regular perturbation expansion (cf. Bird and Warner, 1971; Schiek and Shaqfeh, 1995)

$$
P = P^{[0]} + (Pe)P^{[1]} + (Pe)^2 P^{[2]} + \cdots. \tag{32}
$$

The lowest order distribution is constant,

$$P^{[0]} \equiv 1, \tag{33}$$

and successive corrections are governed by the respective inhomogeneous boundary-value problems

$$\begin{aligned}
&\nabla_g \cdot \left({}^g\mathsf{D} \cdot \nabla_g P^{[k]}\right) = \nabla_g \cdot ({}^g U P^{[k-1]}), \quad (z, \boldsymbol{e}) \in \Omega^{z\boldsymbol{e}}, \\
&(\nabla_g S) \cdot {}^g\mathsf{D} \cdot \nabla_g P^{[k]} = (\nabla_g S) \cdot {}^g U P^{[k-1]}, \quad (z, \boldsymbol{e}) \in \partial\Omega^{z\boldsymbol{e}}, \\
&(\nabla_g z) \cdot {}^g\mathsf{D} \cdot \nabla_g P^{[k]} \to (\nabla_g z) \cdot {}^g U P^{[k-1]}, \quad z \to \infty,
\end{aligned} \tag{34}$$

together with periodicity and boundedness conditions. Here ∇_g, ${}^g\mathsf{D}$, and ${}^g\boldsymbol{U}$ represent shorthand for the "grand" (combined position- and orientation-space) gradient operator, diffusion dyadic, and solute velocity, namely,

$$\nabla_g = (\nabla_z, \nabla_e), \quad {}^g\mathsf{D} = \begin{pmatrix} {}^{zz}\mathsf{D} & {}^{ez}\mathsf{D}^{\dagger} \\ {}^{ez}\mathsf{D} & {}^{ee}\mathsf{D} \end{pmatrix}, \quad {}^g\boldsymbol{U} = \begin{pmatrix} k\dot{z} \\ \dot{\boldsymbol{e}} \end{pmatrix}. \tag{35}$$

The transport equation in Eq. 34 represents the Euler–Lagrange equation for the functional

$$I = \int_{\Omega^{z\boldsymbol{e}'}} \left(\nabla_g P^{[k]} - {}^g\boldsymbol{g}\right) \cdot {}^g\mathsf{D} \cdot \left(\nabla_g P^{[k]} - {}^g\boldsymbol{g}\right) dz\, d^2\boldsymbol{e}, \tag{36}$$

where

$${}^g\boldsymbol{g} = {}^g\mathsf{D}^{-1} \cdot {}^g U P^{[k-1]}, \tag{37}$$

and the auxiliary conditions are natural boundary conditions for the differential operator (cf. Carrier and Pearson, 1976). Thus, solving Eq. 34 is equivalent to minimizing I (cf. Phillips et al., 1989, 1990). The prime in $\Omega^{z\boldsymbol{e}'}$ indicates the fact that, for numerical purposes, the configuration space is truncated above at a sufficiently large finite elevation $z = z_{\max}$.

In order to develop a numerical approximation for $P^{[k]}$, this distribution is expanded as a finite sum

$$P^{[k]} = \sum_{p=0}^{P} \sum_{n=0}^{N} \sum_{m=0}^{2n} C_{mnp} \Phi_{mnp}(z, \theta, \phi), \tag{38}$$

where

$$\begin{aligned}
&\Phi_{mnp}(z, \theta, \phi) \\
&\quad = P_{2n}^{m}(\cos\theta)\cos(m\phi)\cos[p\pi(z - z_{\max})/2z_{\max}].
\end{aligned} \tag{39}$$

The restriction to only cosinusoidal terms in ϕ and even Legendre polynomials follows from the symmetry properties of $P^{[k]}$, namely,

$$\begin{aligned}
P^{[k]}(\theta, \phi, z) &= P^{[k]}(\theta, -\phi, z), \\
P^{[k]}(\theta, \phi, z) &= P^{[k]}(\pi - \theta, \pi + \phi, z).
\end{aligned} \tag{40}$$

Minimization of I then leads to a linear system of the form

$$\sum_{mnp} A_{m'n'p',mnp} C_{mnp} = B_{m'n'p'} \tag{41}$$

for the coefficients C_{mnp}, where

$$\begin{aligned}
A_{m'n'p',mnp} &= \int_{\Omega^{z\boldsymbol{e}'}} \nabla_g \Phi_{m'n'p'} \cdot {}^g\mathsf{D} \cdot \nabla_g \Phi_{mnp}\, dz\, d^2\boldsymbol{e}, \\
B_{m'n'p'} &= \int_{\Omega^{z\boldsymbol{e}'}} \nabla_g \Phi_{m'n'p'} \cdot {}^g U P^{[k-1]}\, dz\, d^2\boldsymbol{e}.
\end{aligned} \tag{42}$$

These integrals are approximated numerically using Simpson's rule. Equation 41 for $m' = n' = p' = 0$ degenerates to $0 = 0$ and is replaced by $\sum_p C_{00p} = 0$ for consistency with Eq. 9 and the fact that Péclet number corrections in P_∞ have zero mean.

Calculations are performed with $z_{\max} = 4$ and $N = 3$, $P = 6$. These values of the numerical parameters yield satisfactory convergence of the distribution function with increasing z and with increasing number of modes. However, since we desire very high accuracy in carrying out our perturbation expansion (Eq. 32) through fourth order for the nonhydrodynamically interacting dumbbell, calculations for this case (and this case exclusively) are performed using more angular modes ($N = 4$). For the dumbbell with hydrodynamic interactions, we evaluate hydrodynamic coefficients for particle–wall contact configurations at a slightly increased (by 10^{-3}) elevation, or else truncate the configuration space at a distance 10^{-3} above the true contact surface given by $S(z, \theta) = 0$, in order to avoid numerical overflow errors associated with the lubrication singularity in the sphere–plane drag coefficients. The calculated distributions are insensitive to the size of the added gap or the precise way in which the gap is introduced.

Distribution over Positions and Orientations

Nonhydrodynamically interacting dumbbell in unbounded shear flow

Results are discussed most rationally with reference to the case of unbounded shear flow. Therefore, it is worthwhile to review briefly the properties of $P_\infty(\boldsymbol{e})$.

The velocity components comprising $\dot{\boldsymbol{e}}$ were given long ago by Jeffery (1922) for spheroidal particles. The dimensionless angular velocity $\dot{\boldsymbol{e}}$ of a dumbbell (with beads that do not interact hydrodynamically) can be obtained from Jeffery's results by considering the aspect ratio to be infinite, or else by direct calculation (cf. Eq. 17); one finds (cf. Bird and Warner, 1971; Jeffery, 1922; Hinch and Leal, 1972; Park and Fuller, 1984; Nitsche and Brenner, 1990)

$$\dot{\boldsymbol{e}} = \boldsymbol{i}_\theta \cos^2\theta \cos\phi - \boldsymbol{i}_\phi \cos\theta \sin\phi. \tag{43}$$

The successive corrections $P_\infty^{[k]}$ in the small Péclet number expansion

$$P_\infty(\boldsymbol{e}) = 1 + (Pe) P_\infty^{[1]}(\boldsymbol{e}) + (Pe)^2 P_\infty^{[2]}(\boldsymbol{e}) + \cdots \tag{44}$$

are determined by the sequence of orientational problems

$$\nabla_e^2 P_\infty^{[k]} = 2\nabla_e \cdot (\dot{\boldsymbol{e}} P_\infty^{[k-1]}). \tag{45}$$

The first two are given explicitly by (cf. Bird and Warner, 1971)

$$P_\infty^{[1]} = (1/3)P_2^1(\cos\theta)\cos\phi,$$

$$P_\infty^{[2]} = (-1/7)P_2^0(\cos\theta) - (2/35)P_4^0(\cos\theta) \qquad (46)$$
$$+ (5/126)P_2^2(\cos\theta)\cos 2\phi + (1/210)P_4^2(\cos\theta)\cos 2\phi.$$

The simple shear flow, Eq. 1, represents a superposition of an elongational flow (with axis of elongational $z = x$ corresponding to $\varphi = \pi/4$, $\vartheta = \pi/2$) and a pure rotation (about the y-axis) (cf. Russel et al., 1989, p. 27). The first-order correction $P_\infty^{[1]}$ manifests a bias toward orientations aligned with the axis of elongation and away from orientations aligned with the perpendicular axis ($z = -x$, or $\varphi = 3\pi/4$, $\vartheta = \pi/2$) (see Figure 5). Only at second order is there a tendency for alignment in the flow direction (see Figure 6).

Nonhydrodynamically interacting dumbbell near a wall

Although the bead radius could be set to zero without loss of generality in this case, calculations are performed with $a = 0.2\ l$ in order to maintain a direct geometrical correspondence with subsequent calculations incorporating bead–bead and bead–wall hydrodynamic interactions.

Figures 5 and 6 compare the corrections $P^{[1]}$ and $P^{[2]}$ at three fixed elevations ($z = 4$, $z = 1.25$, and $z = 0.7$) with the corresponding unbounded-fluid orientational distributions $P_\infty^{[1]}$ and $P_\infty^{[2]}$. Both $P^{[1]}$ and $P^{[2]}$ are essentially indistinguishable from their unbounded-fluid counterparts at $z = 4$. Closer to the wall the variations of $P^{[1]}$ and $P^{[2]}$ at fixed z are smaller than the variations of $P_\infty^{[1]}$ and $P_\infty^{[2]}$. For example, at $z = 1.25$ the amplitude of $P^{[1]}$ is diminished by about 20% (see Figure 5). Thus, the dynamical consequence of steric constraints imposed by the wall is an impediment to the shear-induced solute alignment. This effect, which we shall call "steric damping," seems to decay exponentially with increasing distance from the wall.

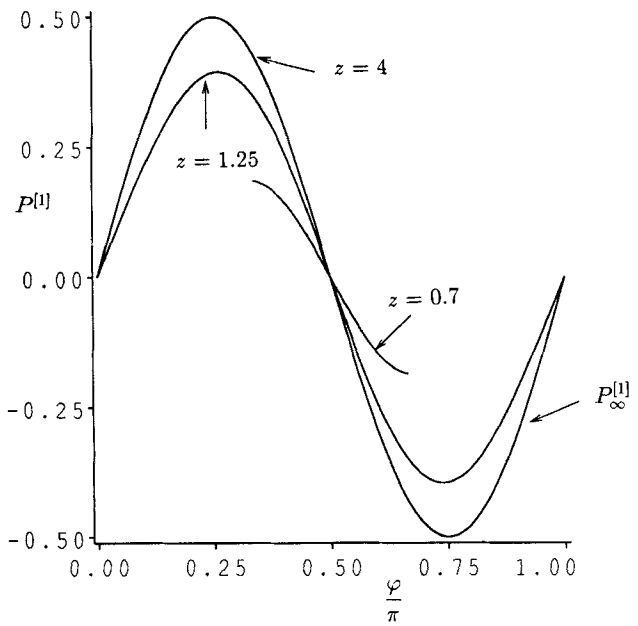

Figure 5. Angular dependence of the first-order configurational distribution $P^{[1]}$ for a dumbbell having $a/l = 0.2$, neglecting hydrodynamic interaction effects.

The dashed curve represents the case of unbounded shear flow, and the solid curves apply to three elevations z above the wall. Not all orientations are accessible at $z = 0.7$. Orientations are in the plane of shear, that is, ϑ is fixed at $\pi/2$.

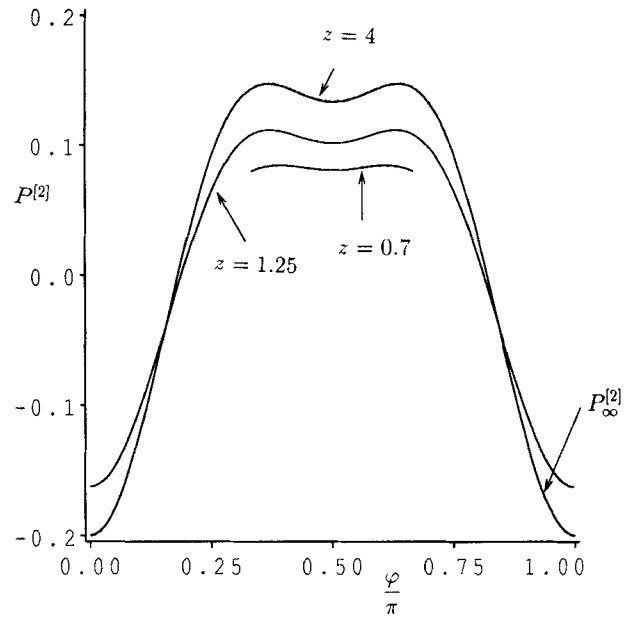

(a)

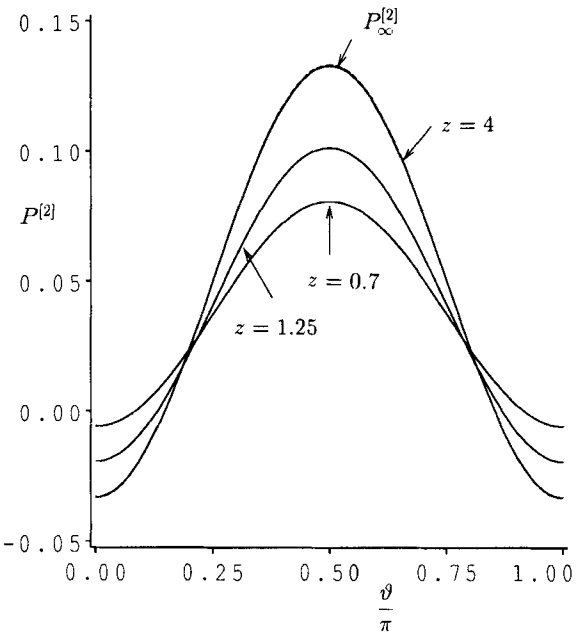

(b)

Figure 6. Angular dependence of the second-order configurational distribution $P^{[2]}$ for a dumbbell having $a/l = 0.2$, neglecting hydrodynamic interaction effects.

The dashed curve represents the case of unbounded shear flow, and the solid curves apply to three elevations z above the wall. Not all orientations are accessible at $z = 0.7$. (a) Orientations in the plane of shear, that is, ϑ fixed at $\pi/2$. (b) Orientations in a horizontal plane normal to the plane of shear, that is, φ fixed at $\pi/2$.

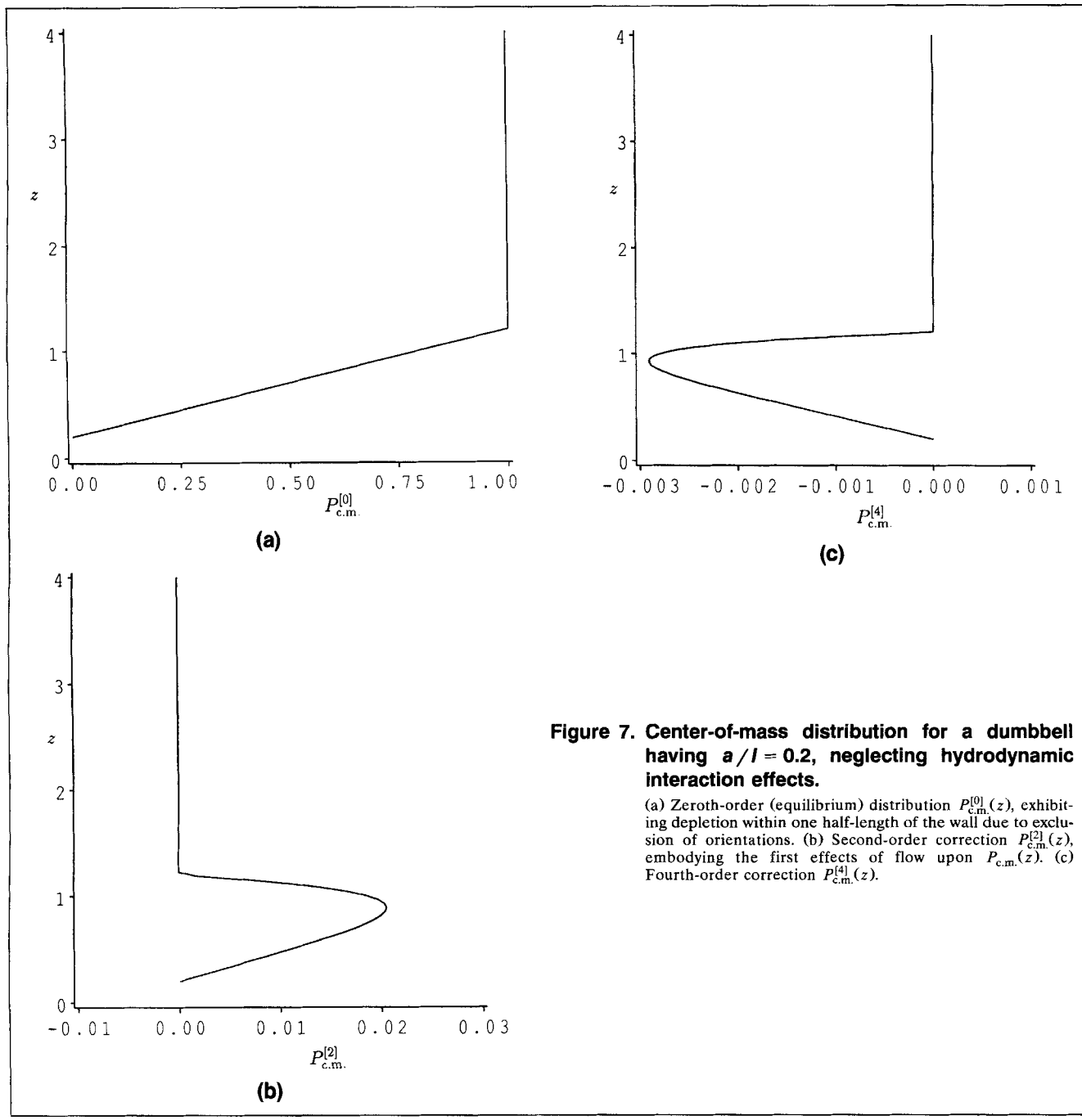

Figure 7. Center-of-mass distribution for a dumbbell having $a/l = 0.2$, neglecting hydrodynamic interaction effects.

(a) Zeroth-order (equilibrium) distribution $P^{[0]}_{c.m.}(z)$, exhibiting depletion within one half-length of the wall due to exclusion of orientations. (b) Second-order correction $P^{[2]}_{c.m.}(z)$, embodying the first effects of flow upon $P_{c.m.}(z)$. (c) Fourth-order correction $P^{[4]}_{c.m.}(z)$.

We carried out the perturbation expansion (Eq. 32) numerically through fourth order in the rotational Péclet number. The overall character of the distribution over accessible configurations is shown by the center-of-mass distribution

$$P_{c.m.}(z) = (4\pi)^{-1}\int_0^{2\pi}\int_{\theta_{min}}^{\pi-\theta_{min}} P(z,\theta,\phi)\sin\theta\, d\theta\, d\phi$$
$$= P^{[0]}_{c.m.}(z) + (Pe)^2 P^{[2]}_{c.m.}(z) + (Pe)^4 P^{[4]}_{c.m.}(z) + O[(Pe)^6] \quad (47)$$

to which only the even terms contribute, the odd terms having zero orientation average. Here,

$$\theta_{min} = \begin{cases} \text{Arccos}\sqrt{[(z-\alpha)^2-\beta^2]/(1-\beta^2)}\,, & z < 1+\alpha, \\ 0 & z \geq 1+\alpha. \end{cases} \quad (48)$$

At lowest order the distribution is unaffected by the flow and is therefore uniform over all accessible positions and orientations ($P^{[0]} \equiv 1$). Owing to the steric preclusion of certain orientations when the dumbbell center lies within one half-length of the wall, $P^{[0]}_{c.m.}(z)$ exhibits a well-known depletion near the wall (DiMarzio and Guttman, 1970; Park and Fuller, 1984; Hoagland, 1988; Ausserré et al., 1991; de Pablo and Öttinger, 1992; Schiek and Shaqfeh, 1995; cf. Aubert and Tir-

rell 1982) (Figure 7a). Figures 7b and 7c show second- and fourth-order corrections to $P_{c.m.}(z)$. As expected, alignment with the flow (manifested in $P_{\infty}^{[2]}$ and $P^{[2]}$) has the consequence that the dumbbell can get closer to the wall. Thus, the first flow effect is to partially counteract the zeroth-order (equilibrium) depletion (Figure 7b). However, the fourth-order correction tends to reinforce the depletion (Figure 7c).

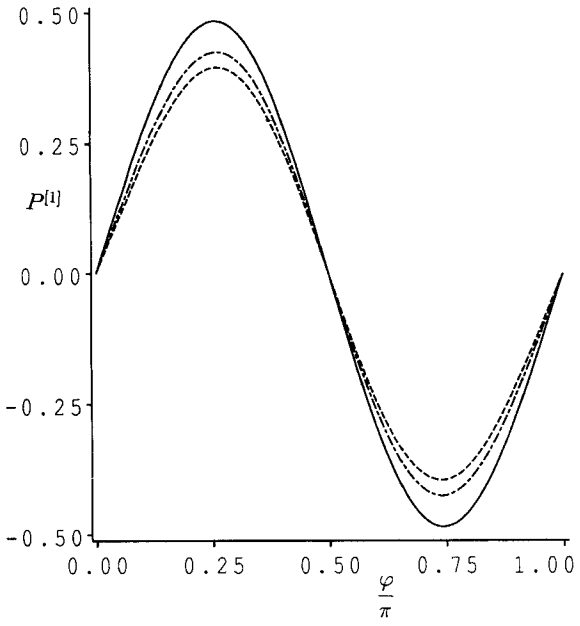

(a)

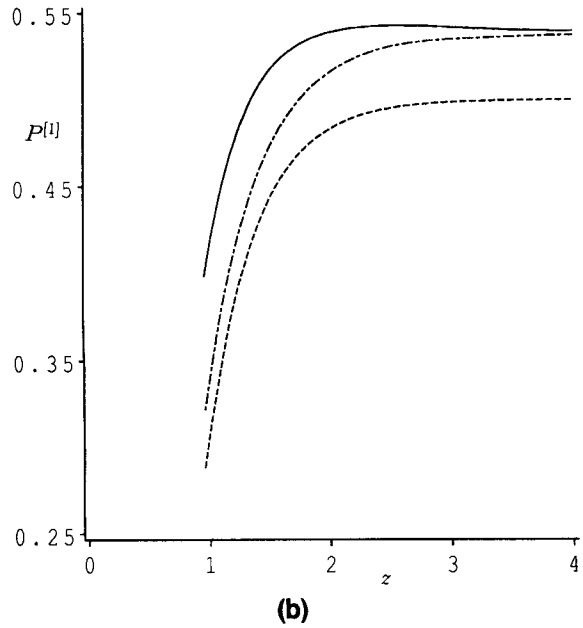

(b)

Figure 8. First-order configurational distribution $P^{[1]}$ for a dumbbell having $a/l = 0.2$.

Dashed curves—no interactions; dot-dashed curves—only bead—bead interactions switched on; solid curves—both bead—bead and bead—wall interactions switched on. (a) Angular (φ) dependence in the plane of shear ($\vartheta = \pi/2$) at elevation $z = 1.25$. (b) z Dependence at orientation $\vartheta = \pi/2$, $\varphi = \pi/4$, the most probable orientation in unbounded shear flow.

Hydrodynamically Interacting Dumbbell Near a Wall

To compare the effects of bead–bead interactions (present even in unbounded shear flow) and hydrodynamic wall effects, Figures 8 and 9 show results for three versions of the dumbbell: (1) the noninteracting dumbbell (dashed curves); (2) a dumbbell with bead–bead hydrodynamic interactions switched on, but bead–wall interactions switched off (dot-dashed curves); and (3) a dumbbell with full accounting for both bead–bead and bead–wall hydrodynamic interactions (solid curves). Aside from observing generally that both bead–bead and bead–wall hydrodynamic interactions change the distribution function quantitatively, two broad conclusions can be drawn from these figures by comparing solutes (2) and (3). First, hydrodynamic interactions with the wall increase the amplitude of the angular variations of P at small z. As is evident from Figure 8a, the increase for $P^{[1]}$ amounts to about 15% at $z = 1.25$. An explanation for this phenomenon can be formulated with reference to Figures 3a and 3b. Since hydrodynamic interactions have little influence upon the angular velocity but significantly decrease the rotary diffusivity near the wall, they locally increase the effective rotary Péclet number (effective flow strength), and thereby the amplitudes of the $P^{[k]}$. The magnitude of the increase of $k = 1$ is roughly consistent with the decrease in rotary diffusivity manifested in Figure 3b. (A comparison between solutes (1) and (2) reinforces this explanation: solute (2) has the smaller rotary diffusivity and, correspondingly, the larger amplitude of $P^{[1]}$.) It is thus interesting to note that solute–wall hydrodynamic interactions partly counteract the steric damping effect. Second, this phenomenon makes the second-order center-of-mass accumulation near the wall (which opposes the equilibrium depletion) more pronounced, although there is now a slight dip above $z = 1$; the maximum value of $P_{c.m.}^{[2]}(z)$ increases by about 15%.

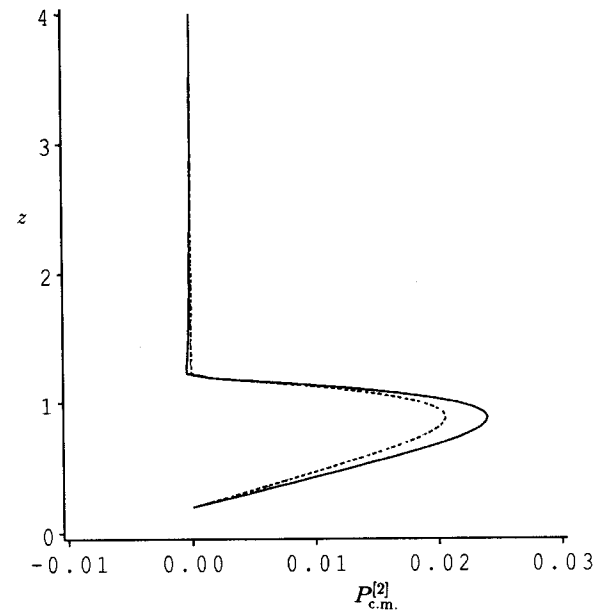

Figure 9. Second-order correction $P_{c.m.}^{[2]}(z)$ to the center-of-mass distribution for a dumbbell having $a/l = 0.2$; significance of curves is as in Figure 8.

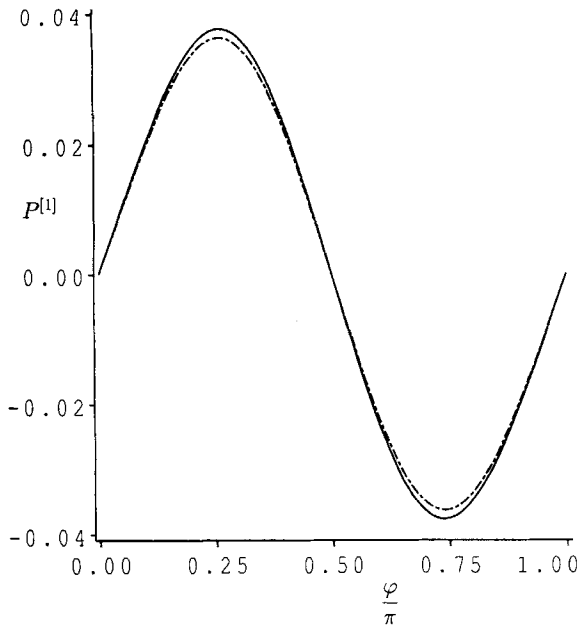

(a)

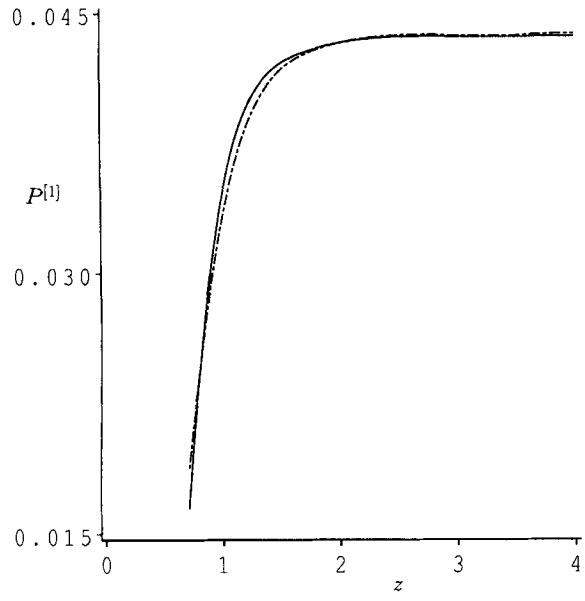

(b)

Figure 10. First-order configurational distribution $P^{[1]}$ for a spheroid having aspect ratio $\beta = 0.1$.

Dot-dashed curves—hydrodynamic wall effects switched off; solid curves—hydrodynamic wall effects switched on. (a) Angular (φ) dependence in the plane of shear ($\vartheta = \pi/2$) at elevation $z = 1.1$. (b) z Dependence at orientation $\vartheta = \pi/2$, $\varphi = \pi/4$.

A close examination of Figure 8b indicates that, in the presence of bead–wall hydrodynamic interactions, the first-order correction $P^{[1]}$ at a fixed orientation goes through a weak maximum around $z = 2.5$. This feature of $P^{[1]}$ is explicable in view of Figure 3c. At the orientation considered, the force- and torque-free convective velocity has a significant downward component. This tends to cause an accumulation of dumbbell configurations at smaller z (akin to a gravitational Boltzmann bias), but is overpowered by the decrease in

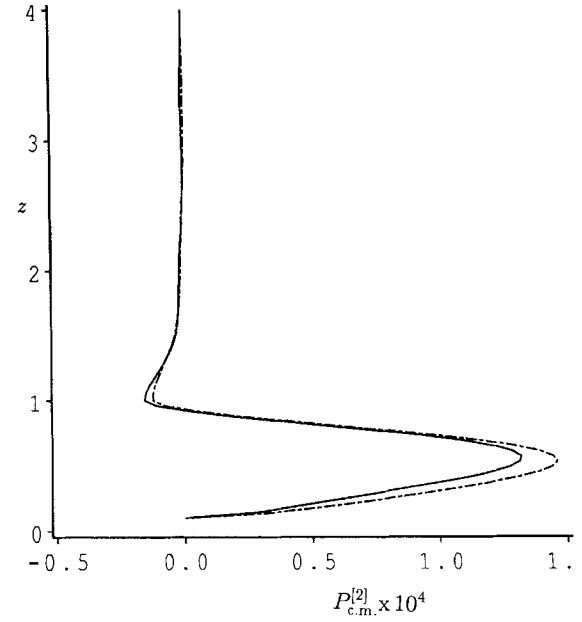

Figure 11. Second-order correction $P^{[2]}_{c.m.}(z)$ to the center-of-mass distribution for a spheroid having aspect ratio $\beta = 0.1$; significance of curves is as in Figure 10.

amplitude (steric damping effect) as $z \to 0$ (cf. Figure 5), hence the maximum at a finite value of z.

Spheroid Near a Wall

Figures 10 and 11 show corresponding results for a spheroid with aspect ratio $\beta = 0.1$. Analogously to (2) and (3), the dot-dashed curves represent the case where hydrodynamic wall effects are artificially switched off and the solid curves represent the full solution embodying hydrodynamic interactions with the wall. Although there are quantitative differences, the preceding overall qualitative conclusions are confirmed. Details of the distribution function at small z must be regarded as suspect because our hydrodynamic approximations for the spheroid underestimate the severity of hindrance effects near the wall.

Discussion

Preceding calculations represent a detailed investigation of the manner in which steric and hydrodynamic wall effects influence the configurational distributions of nonspherical particles in shear flow near a wall. Steric constraints tend to damp angular variations in the distribution function, impeding shear-induced alignment relative to the case of unbounded fluid. In constrast, hydrodynamic interactions with the wall increase the amplitude of angular variations owing to an effective local increase in the rotational Péclet number. The magnitude of these changes in the distribution function is of order 15–20% for the dumbbell at $z = 1.25$. Although addressing the simplest (plane wall, constant shear) system, the results and conclusions regarding near-wall physics apply generally (e.g., to pressure-driven flows through pores) insofar as the wall appears locally flat and the flow is locally linear. The consideration (albeit approximate) of both dumb-

bell-shaped and spheroidal solutes collectively addresses both lubrication effects (by the inclusion of exact sphere–plane interactions in the case of the dumbbell) and realistic representation of rodlike solute shapes (for the spheroid).

Schiek and Shaqfeh's (1995) Figure 5 indicates that their $P^{[2]}_{\text{c.m.}}(z)$ is positive for $0 < z < 0.5$, but negative for $0.5 < z < 1$ (and zero for $z > 1$). The infinitesimally thin rodlike solute studied by them most closely resembles the spheroid model with hydrodynamic wall effects switched off (dot-dashed curves in Figures 10 and 11). Our $P^{[2]}_{\text{c.m.}}(z)$ for this solute is positive over most of the interval $0 < z < 1$, with only a slight dip to negative values near $z = 1$ (which, in fact, extends to elevations above $z = 1$). This difference in behavior may be a consequence of the nonlinearity of Schiek and Shaqfeh's fluid velocity profile, which arises from their consideration of the effect of solutes upon the fluid stress.

Simulations of de Pablo et al. (1992) show that flow counteracts the equilibrium depletion near the wall at low shear rates, but reinforces this depletion at high shear rates. (The predicted high-shear rate trend seems to be observed experimentally (Ausserré et al., 1991), as is noted by de Pablo et al.) Insofar as a small Peclet number expansion serves to ascertain the full Péclet number dependence of the solute center-of-mass concentration, our findings are suggestive of the same conclusion, because $P^{[2]}_{\text{c.m.}}(z)$ is predominantly negative but $P^{[4]}_{\text{c.m.}}(z)$ is positive.

Acknowledgments

Financial support of this work through an NSF Young Investigator Award to one of the authors (J.M.N.) and through grants from the American Chemical Society Petroleum Research Fund and the Proctor & Gamble Company is gratefully acknowledged. The authors take pleasure in thanking Prof. Juan José de Pablo for a useful discussion, and the anonymous reviewers of the manuscript for helpful comments.

Notation

$A_{m'n'p',mnp}, B_{m'n'p'}$ = matrix and righthand side of linear system that determines the coefficients C_{mnp}
C_{mnp} = coefficient in series expansion for kth-order distribution function $P^{[k]}$
D_∞ = scalar with dimensions of a translation diffusivity
$^t\mathsf{D}$ = translational diffusion dyadic
$^c\mathsf{D}$ = diffusion dyadic for coupling between translational and rotational motions
$^r\mathsf{D}$ = rotational diffusion dyadic
$G_\parallel, G_\perp$ = dimensionless translational resistance coefficients for spheroid in unbounded fluid
I = unit isotropic dyadic
$H_\parallel, H_\perp$ = dimensionless rotational resistance coefficients for spheroid in unbounded fluid
$\boldsymbol{i}, \boldsymbol{j}, \boldsymbol{k}$ = orthonormal triad of space-fixed coordinate unit vectors
$\boldsymbol{i}_\theta, \boldsymbol{i}_\phi, \boldsymbol{e}$ = solute-fixed orthonormal triad
$^t\mathsf{K}$ = translation resistance dyadic
$^c\mathsf{K}$ = resistance dyadic for coupling between translational and rotational motions
$^r\mathsf{K}$ = rotational resistance dyadic
K_∞ = translational resistance dyadic for spheroid in unbounded fluid
kT = Boltzmann factor
l = half-length of dumbbell
$P^{[k]}(z, \theta, \phi)$ = kth-order correction in regular perturbation expansion for $P(z, \theta, \phi)$
$\dot{z}$ = z component of solute translational velocity $\boldsymbol{U}$
α = aspect ratio of dumbbell
β = aspect ratio of spheroid
$\dot{\gamma}$ = shear rate
∇_x = position-space gradient operator
∇_e = orientation-space gradient operator
μ = fluid viscosity

Superscript

$[k]$ = order in perturbation expansion

Literature Cited

Aubert, J. H., and M. Tirrell, "Effective Viscosity of Dilute Polymer Solutions near Confining Boundaries," *J. Chem. Phys.*, **77**, 553 (1982).
Ausserré, D., J. Edwards, J. Lecourtier, H. Hervet, and F. Rondelez, "Hydrodynamic Thickening of Depletion Layers in Colloidal Solutions," *Europhys. Lett.*, **14**, 33 (1991).
Bird, R. B.,and H. R. Warner, Jr., "Hydrodynamic Interaction Effects in Rigid Dumbbell Suspensions. I. Kinetic Theory," *Trans. Soc. Rheol.*, **15**, 741 (1971).
Blake, J. R., "A Note on the Image System for a Stokeslet in a No-Slip Boundary," *Proc. Cambridge Phil. Soc.*, **70**, 303 (1971).
Brenner, H., "The Slow Motion of a Sphere through a Viscous Fluid Towards a Plane Surface," *Chem. Eng. Sci.*, **16**, 242 (1961).
Brenner, H., "Effect of Finite Boundaries on the Stokes Resistance of an Arbitrary Particle," *J. Fluid Mech.*, **12**, 35 (1962).
Brenner, H. and D. W. Condiff, "Transport Mechanics in Systems of Orientable Particles. III. Arbitrary Particles," *J. Colloid Interface Sci.*, **41**, 228 (1972).
Brunn, P. O., and S. Grisafi, "Wall Effects in Simple Shear of Dilute Polymer Solution: Exact Results for Very Narrow and Very Wide Channels," *J. Non-Newtonian Fluid Mech.*, **24**, 343 (1987a).
Brunn, P. O., and S. Grisafi, "Pressure Driven Flow of Dilute Polymer Solutions in a Channel: Analytic Results for Very Small and Very Large Channels," *Rheol. Acta*, **26**, 211 (1987b).
Carrier, G. F., and C. E. Pearson, "Partial Differential Equations: Theory and Technique, Chap. 10, Academic Press, New York (1976).
Chauveteau, G., "Rodlike Polymer Solution Flow Through Fine Pores: Influence of Pore Size on Rheological Behavior," *J. Rheol.*, **26**, 111 (1982).
Condiff, D. W., and J. S. Dahler, "Brownian Motion of Polyatomic Molecules: The Coupling of Rotational and Translational Motions," *J. Chem. Phys.*, **44**, 3988 (1966).
de Pablo, J. J., H. C. Öttinger, and Y. Rabin, "Hydrodynamic Changes of the Depletion Layer of Dilute Polymer Solutions Near a Wall," *AIChE J.*, **38**, 273 (1992).
DiMarzio, E. A., and C. M. Guttman, "Separation by Flow," *Macromolecul*, **3**, 131 (1970).
Falade, A., and H. Brenner, "Stokes Wall Effects for Particles Moving Near Cylindrical Boundaries," *J. Fluid Mech.*, **154**, 145 (1985).
Falade, A., and H. Brenner, "First-order Wall Curvature Effects upon the Stokes Resistance of a Spherical Particle Moving in Close Proximity to a Solid Wall," *J. Fluid Mech.*, **193**, 533 (1988).
Giddings, J. C., "Field-flow Fractionation," *Sep. Sci. Technol.*, **19**, 831 (1984–1985).
Goh, C. J., J. D. Atkinson, and N. Phan-Thien, "The Flow of Dilute Polymer Solution in a Narrow Channel: I. The Slip Effect in Simple Shear Flow," *J. Chem. Phys.*, **82**, 988 (1985a).
Goh, C. J., J. D. Atkinson, and N. Phan-Thien, "The Flow of Dilute Polymer Solution in a Narrow Channel. II. Plane Poiseuille Flow," *J. Chem. Phys.*, **82**, 3442 (1985b).
Goldman, A. J., R. G. Cox, and H. Brenner, "Slow Viscous Motion of a Sphere Parallel to a Plane Wall—I. Motion through a Quiescent Fluid," *Chem. Eng. Sci.*, **22**, 637 (1967a).
Goldman, A. J., R. G. Cox, and H. Brenner, "Slow Viscous Motion of a Sphere Parallel to a Plane Wall—II. Couette Flow," *Chem. Eng. Sci.*, **22**, 653 (1967b).
Grisafi, S., and P. O. Brunn, "Wall Effects in the Flow of a Dilute Polymer Solution: Numerical Results for Intermediate Channel Sizes," *J. Rheol.*, **33**, 47 (1989).
Happel, J., and H. Brenner, *Low Reynolds Number Hydrodynamics*, Kluwer, Boston (1991).
Hinch, E. J., and L. G. Leal, "The Effect of Brownian Motion on the

Table A1. Notational Equivalences for Hydrodynamic Problems Involving Motion of or Flow Past a Sphere Near a Plane Wall

Investigation	Dimensionless Force Due to Translation ∥ to Wall	Dimensionless Force Due to Translation ⊥ to Wall	Dimensionless Torque Due to Rotation about Axis ∥ to Wall	Dimensionless Torque Due to Translation ∥ to Wall	Dimensionless Force Due to Shear Flow	Dimensionless Torque Due to Shear Flow
Brenner (1961)		λ				
Goldman et al. (1967a)	$-F_x^{t*}$		$-T_y^{r*}$	T_y^{t*}		
Goldman et al. (1967b)					F_x^{s*}	T_y^{s*}
Falade and Brenner (1988)	a	b	c	e		

Rheological Properties of a Suspension of Non-Spherical Particles," *J. Fluid Mech.*, **52**, 683 (1972).

Hirschfeld, B. R., H. Brenner, and A. Falade, "First- and Second-order Wall Effects upon the Slow Viscous Asymmetric Motion of an Arbitrarily-Shaped, -Positioned and -Oriented Particle within a Circular Cylinder," *PhysicoChem. Hydrodyn.*, **5**, 99 (1984).

Hoagland, D. A., "Concentration Profiles of Rod-like Polymers in Narrow Channels," *J. Colloid Interface Sci.*, **123**, 117 (1988).

Hsu, R., and P. Ganatos, "The Motion of a Rigid Body in Viscous Fluid Bounded by a Plane Wall," *J. Fluid Mech.*, **207**, 29 (1989).

Ingber, M. S., and L. A. Mondy, "A Numerical Study of Three-Dimensional Jeffery Orbits in Shear Flow," *J. Rheol.*, **38**, 1829 (1994).

Jeffery, G. B., "The Motion of Ellipsoidal Particles Immersed in a Viscous Fluid," *Proc. Roy. Soc. London, Ser. A*, **102**, 161 (1922).

McHugh, A. J., "Particle Size Measurement Using Chromatography," *CRC Crit. Rev. Analyt. Chem.*, **15**, 63 (1984).

Nadim, A., and H. Brenner, "Long-time Nonpreaveraged Diffusion and Sedimentation Properties of Flexible Brownian Dumbbells, " *PhysicoChem. Hydrodyn.*, **11**, 315 (1989).

Nitsche, J. M., "Pore Diffusion of Nonspherical Brownian Particles," *Ind. Eng. Chem. Res.*, **34**, 3606 (1995).

Nitsche, J. M., "Hydrodynamic Coupling and Nonequilibrium Distribution in Pore Diffusion of Nonspherical Fine Particles," *Particulate Sci. Technol.*, **9**, 135 (1991).

Nitsche, J. M., and G. Balgi, "Hindered Brownian Diffusion of Spherical Solutes within Circular Cylindrical Pores," *Ind. Eng. Chem. Res.*, **33**, 2242, 2246 (1994).

Nitsche, J. M., and H. Brenner, "On the Formulation of Boundary Conditions for Rigid Nonspherical Brownian Particles near Solid Walls: Applications to Orientation-Specific Reactions with Immobilized Enzymes," *J. Colloid Interface Sci.*, **138**, 21 (1990).

Park, O. O., and G. G. Fuller, "Dynamics of Rigid and Flexible Polymer Chains in Confined Geometries. Part I: Steady Simple Shear Flow," *J. Non-Newtonian Fluid Mech.*, **15**, 309 (1984).

Phillips, R. J., J. F. Brady, and W. M. Deen, "Hindered Transport of Spherical Macromolecules in Fibrous Membranes and Gels," *AIChE J.*, **35**, 1761 (1989).

Phillips, R. J., J. F. Brady, and W. M. Deen, "Hindered Transport in Fibrous Membranes and Gels: Effect of Solute Size and Fiber Configuration," *J. Colloid Interface Sci.*, **139**, 363 (1990).

Prud'homme, R. K., G. Froiman, and D. A. Hoagland, "Molecular Size Determination of Xanthan Polysaccharide," *Carbohydr. Res.*, **106** 225 (1982).

Prud'homme, R. K., and D. A. Hoagland, "Orientation of Rigid Macromolecules during Hydrodynamic Chromatography Separations," *Sep. Sci. Technol.*, **18**, 121 (1983).

Russel, W. B., D. A. Saville, and W. R. Schowalter, *Colloidal Dispersions*. Cambridge Univ. Press, New York p. 27 (1989).

Schiek, R., and E. S. G. Shaqfeh, "A Nonlocal Theory for Stress in Bound, Brownian Suspensions of Slender, Rigid Fibres," *J. Fluid Mech.*, **296**, 271 (1995).

Stasiak, W., and C. Cohen, "Dilute Solutions of Macromolecules in a Rectilinear Poiseuille Flow," *J. Chem. Phys.*, **78**, 553 (1983).

Stewart, W. E., and J. P. Sorensen, "Hydrodynamic Interaction Effects in Rigid Dumbbell Suspensions. II. Computations for Steady Shear Flow," *Trans. Soc. Rheol.*, **16**, 1 (1972).

Stover, C. A., and C. Cohen, "The Motion of Rodlike Particles in the Pressure-Driven Flow Between Two Flat Plates," *Rheol. Acta*, **29**, 192 (1990).

Appendix: Hydrodynamic Inputs for the Dumbbell

Since we draw from a number of results for sphere–wall hydrodynamic interaction in calculating the direct bead resistance dyadics k_{++} and k_{--} according to Eq. 14, it is worthwhile to present some details of the calculations and to establish correspondences between notation schemes employed in the articles cited.

To calculate the hydrodynamic coefficients entering $F_{\parallel}$ and $F_{\perp}$ we utilize far-field asymptotic expressions for $z_{\pm}/a > 10.0677$, interpolation for $10.0677 \geq z_{\pm}/a \geq 1.003202$, and lubrication-theory asymptotes for $1.003202 > z_{\pm}/a > 1$. Our routines collect the numerical values and asymptotic formulas listed by Brenner (1961), Goldman et al. (1967a), and Falade and Brenner (1988). In the intermediate regime our interpolation is linear in a table giving the hydrodynamic coefficients as a function of $\ln[(z_{\pm}/a)-1]$. The only exception is the coefficient b or λ, for which we use $\ln b = \ln \lambda$ instead of $b = \lambda$ itself. A few errata in the tabulation of Falade and Brenner (1988) have been corrected (cf. Nitsche and Balgi, 1994). The functions $F_{\parallel}$ and $F_{\perp}$ are given explicitly by the following expressions (see Table A.1):

$$F_{\parallel} = a - (4/3)e^2/c,$$
$$F_{\perp} = b = \lambda. \tag{49}$$

To calculate the additional hydrodynamic coefficients entering F_s we use the results of Goldman et al. (1967b) in the form of far-field asymptotic expressions for $z_{\pm}/a > 10.0677$, and interpolation for $10.0677 \geq z_{\pm}/a \geq 0$. It is unnecessary to distinguish a third small-gap interval, as the shear coefficients F_x^{s*} and T_y^{s*} approach finite limits or $z_{\pm}/a \to 1$. Interpolation is linear in a table giving the shear coefficients as functions of $(z_{\pm}/a)^{-1}$. F_s is given explicitly by the equation (Table A1).

$$F_s = F_x^{s*} + (2/3)(z \pm /a)^{-1} T_y^{s*} e/c. \tag{50}$$

Assuming freely rotating beads for the dumbbell model with hydrodynamic wall effects is common (Nadim and Brenner, 1989) and simplifies the hydrodynamic calculations, but is unessential. Coupling between translational and rotational motions leads to only slight numerical differences between translational resistance coefficients of freely rotating and nonfreely rotating spheres near a plane wall (cf. Goldman et al., 1967a).

Manuscript received Mar. 23, 1995, and revision received Feb. 23, 1996.